Experimental Investigations into the Propagation of Acoustic Emission Signals from Particle Impacts along a Waveguide

Authors: Yonghui Hu [a]

Guoqiang Zhang [a] (Corresponding author)

Yong Yan [b]

Addresses: [a] School of Control and Computer Engineering

North China Electric Power University

Beijing 102206

P. R. China

[b] School of Engineering and Digital Arts

University of Kent

Canterbury

Kent CT2 7NT

UK

Tel: +86 01061771330

Email: zhangguoqiang21@ncepu.edu.cn

ABSTRACT

On-line particle sizing through acoustic emission (AE) sensing is promising in many industrial applications. However, very limited research on the fundamental sensing mechanism of this technique is available. One imminent issue is the propagation of impact-induced AE signals along a waveguide, which plays a significant role in interpreting the resulting acoustic waveforms and optimizing the design of the waveguide. In this paper, a broadband point-contact sensor, which has an extremely flat frequency response, is used to acquire faithful AE signals. Experimental investigations into the wave propagation behaviour are presented and the influences of different parameters, including particle size, impact velocity, material type and impact location, on the detected AE signals are also discussed. Two fundamental waves with different characteristics are observed in the acoustic waveforms. Experimental results obtained demonstrate that both the particle size and material type greatly affect the amplitude rather than the signal pattern of the acoustic waveform. Meanwhile, significant changes in the signal amplitude and pattern occur with different impact velocities and impact locations.

Keywords – Wave propagation, acoustic emission, waveguide, particle impact, point-contact sensor.

1. INTRODUCTION

Waveguides are widely utilised for acoustic emission (AE) detection in various industries, such as petrochemical engineering, gas transportation, metal casting and power generation [1-4]. In these cases, it is impossible to place an AE sensor directly on the surface of the examined specimen due to the inaccessible location on structure or the harsh industrial environment [5]. The waveguides for practical AE applications are usually in the form of cylindrical rods or tubes [6]. By guiding the elastic stress waves emitted from an AE event down a waveguide, the AE sensor

can receive signals while mounted conveniently away from the location of AE source. However, during the propagation along a waveguide, the acoustic waves are significantly changed as a result of reflection, attenuation and dispersion, meaning that the waveguide has an important influence on the detected AE signals. Therefore, it is essential to investigate the behaviour of acoustic waves propagating along a waveguide.

For the on-line sizing of pneumatically conveyed particles by AE methods in pulverized fuel fired power plants, a wear-resistant waveguide is protruded into the particle flow through a hole drilled in the pipeline wall [7]. As the AE signals are susceptible to the environmental noise and the continuous vibration of the pneumatic conveying pipelines, the employment of the waveguide can enhance the possibility of signal detection. The basic principle of particle size measurement by AE methods is to establish the relationship between the characteristic parameters of the detected AE signal and the particle size, which is directly related to the collision process (AE source) [8,9]. However, the signals received by the AE sensor have lost fidelity and are severely distorted after propagating along a waveguide, which complicates the interpretation of the AE waveforms [10]. Although preliminary efforts have been carried out to demonstrate the validity of the AE-based particle sizing technique, there is very limited work undertaken to investigate the propagation of acoustic waves arising from collisions along the waveguide, which has hindered further development of this method in terms of measurement accuracy. Besides, the study on the wave propagation is also conducive to the optimized design of the waveguide.

Some attempts have been conducted to interpret the wave propagation behaviour along a waveguide. Sikorska et al. [11,12] carried out experimental work using a series of waveguides with various materials and shapes. In this way, the influences of the waveguide material and shape on the detected AE signals were analysed in both the time and frequency domains. Hamstad [13]

investigated the characteristics of the AE signals acquired with and without a waveguide and found that the diameter of the waveguide affects the duplication of the original AE signal. Vergeynst et al. [14] studied the wave propagation along a cylindrical rod through finite element modelling (FEM). A good agreement was observed between the simulated and measured waveforms. Further investigations were also implemented by changing the angle and distance between the AE source and the surface of the rod. In a similar way, Zelenyak et al. [15] also introduced the FEM to evaluate the propagation of the AE signals along a waveguide. The modal conversion of the AE waveforms was discussed under different simulated conditions. In these studies, pencil lead break (PLB) is usually used as the AE source, which is described by a cosine bell function [16]. However, the impact-induced AE signal has a totally different source, which is the collision between a particle and a waveguide. Different AE sources lead to resulting signals with different characteristics after propagating along a waveguide. And the influences of the parameters (i.e. particle size, impact velocity, material type and impact location) during collision processes on the resulting AE signals are still unclear. In order to obtain a better understanding of the AE-based particle sizing technique, investigations into the propagation of impact-induced AE signals along a waveguide are necessary.

Unlike the existing research which studied the wave propagation with a PLB source, this paper focuses on the propagation behaviour of the AE signals induced by particle impacts, which is a key issue in the particle size measurement through AE sensing but still remains to be examined. As commonly used resonant AE sensors greatly affect the characteristics of the signals being detected, the details of the detected AE signals are altered or lost, which goes against the understanding of wave propagation mechanism along a waveguide. Therefore, a broadband point-contact sensor with an extremely flat frequency response over the operating frequency was

applied to measure the acoustic waveforms generated by free-fall particles impinging onto a waveguide. In this way, the influence of the AE sensor on the detected signals can be minimized and more faithful signals were thus obtained. Glass beads and steel beads with various diameters were used as the test particles. The effects of different parameters, including particle size, impact velocity, particle material and impact location, on the resulting AE signals were experimentally investigated.

2. METHODOLOGY

2.1 General Principle

In a particle sizing system through AE sensing, the signal detected by an AE sensor is not only relevant to the impact dynamics but also to the physics of the elastic wave propagation and the instrument response to the surface disturbance at the detection point. Assuming that both the wave propagation medium and the instrument are modeled as linear-time-invariant systems, the detected AE signal, $V(t)$, can be given in time domain by [17]

$$V(t) = S(t) * G(t) * I(t) \tag{1}$$

where $S(t)$, $G(t)$ and $I(t)$ denote the AE source, wave propagation and instrument response functions, respectively. The symbol * represents convolution.

The $S(t)$ contains all the information concerning the collision process between a particle and a waveguide. The $G(t)$ is the solution of the elastodynamic equations describing the propagation of elastic waves in homogeneous materials, which is called as Green's function. The determination of a quantitative Green's function is very challenging as it is related to the source type, structure geometry and detection point. Theoretical results are only available for some simple geometries, such as a flat plate or a sphere. The $I(t)$ mainly refers to the impulse response of the AE sensor

used in the detection system, which is inevitable in theory but can be minimized by the usage of a high fidelity sensor, such as a broadband point-contact AE sensor.

2.2 Hertzian Impact Theory

The collision between two solid bodies is usually described by the Hertzian impact theory, which assumes the contact is normal and elastic during the impact. Therefore, the AE source representing the collision of a particle onto a plate can be approximated by [18]

$$S(t) = \begin{cases} F_{max} \sin(\frac{\pi t}{T_c})^{\frac{3}{2}} & 0 \le t \le T_c \\ 0 & \text{otherwise} \end{cases} \tag{2}$$

where F_{max} is the maximum contact force during the collision, which is expressed as

$$F_{max} = 0.7574 D^2 K^{\frac{2}{5}} \rho^{\frac{3}{5}} v_0^{\frac{6}{5}} \tag{3}$$

and T_c is the contact time, which is given by

$$T_c = 2.5412 (\frac{\rho}{K})^{\frac{2}{5}} D v_0^{-\frac{1}{5}} \tag{4}$$

where D, ρ and v_0 are the equivalent diameter, mass density and impact velocity of the particle, respectively. K is a constant expressed as

$$K = (\frac{1-\upsilon_1^2}{E_1} + \frac{1-\upsilon_2^2}{E_2})^{-1} \tag{5}$$

where E_i and υ_i (i = 1, 2) are Young's modulus and Poisson's ratio, respectively. Subscript 1 here refers to the particle while subscript 2 represents the plate.

Based on the Hertzian impact theory, the force pulses for different sized glass beads impinging onto a stainless plate at a velocity of 0.5 m/s and 1.0 m/s, respectively, are calculated, as shown in Fig. 1. It can be seen that the contact force during the collision increases with both the particle size and impact velocity, while the contact time increases with the particle size but decreases with

the impact velocity. Although the force pulses are affects by different particle sizes and impact velocities, the patterns of which still show similar tendencies.

3. EXPERIMENTAL METHOD

3.1. Sensing arrangement

The sensing arrangement in an AE-based particle sizing system is schematically illustrated in Fig. 2. An AE sensor is coupled to the outer end of a waveguide, which transforms the elastic stress waves excited by particle collisions into electric signals [19]. In this way, it is convenient to maintain, re-calibrate or replace the AE sensor as needed. Meanwhile, the AE sensor can also be protected from the erosion due to the moving particles. The waveguide with a flat plane is inserted into a vertical pneumatic conveying pipeline line where particles move upwards. At such a location the particle distribution is relatively steady and homogeneous, so we can assume with reasonable confidence that the collisions between the particles and the waveguide take place in the direction normal to the flat plane of the waveguide. In comparison with the dimensions of the pipeline, the width and protruding length of the waveguide is small, which is beneficial to reduce the chance of simultaneous multi-particle collisions and the influence on the particle flow. In addition, as the moving particles collide with the waveguide at different positions, the detected AE signals may also be affected. In order to investigate the propagation of AE signals under different impact conditions, two waveguides with similar geometries of that used in the particle sizing system are employed for conducting the experimental work in this study.

3.2. Experimental setup

Fig. 3(a) shows the schematic diagram of the short waveguide and the mounting positions of the AE sensor. The short waveguide is a stainless-steel probe with a total length of 118 mm, which generally consists of three sections. The first section of the short waveguide is semi-

cylindrical with a 300 mm^2 (30 mm long and 10 mm wide) flat plane, which faces the direction of the particle falling and enables normal particle impact. The semi-cylindrical structure also contributes to prevent the build-up of particles and minimize the turbulence effects due to the intruded waveguide. The middle section is cylindrical with a diameter of 10 mm. The end section of the short waveguide is also semi-cylindrical but with opposite direction of the flat plane, which is 15 mm in length and 10 mm in width. For most experiments, an AE sensor is mounted onto the side of the cylindrical surface (solid lines). In order to investigate the wave modes contained in the AE signal, the same AE sensor is also attached to the side of the flat plane at the opposite position (dotted lines). Meanwhile, another waveguide with a longer length was utilised to study the influence of the impact location on the AE signal, as presented in Fig. 3(b). The long waveguide is also made of stainless steel and has a much longer length of 800 mm. The semi-cylindrical section of the long waveguide is 400 mm long and 10 mm wide. Five different impact locations are chosen and the distance between two adjacent impact locations is 75 mm. An AE sensor is mounted in a similar way to that for the short waveguide, i.e. attached to the cylindrical surface of the long waveguide.

AE sensors have significant influences on the interpretation of the wave propagation. Most AE sensors used in previous studies are resonant sensors or broadband sensors with non-flat frequency response, which strongly affects the time-domain profile and the frequency spectrum of the detected AE signal [20, 21]. Moreover, the sensing area of a common AE sensor is usually a circular plate, over which the stress waves are averaged. As a result, the detected waveforms are distorted [22]. This phenomenon is known as the aperture effect, which can be minimized by the use of an AE sensor with a sensing area as small as possible. The AE sensor (KRNBB-PC, KRN Services) used in this study is a broadband point-contact sensor, which has an extremely flat

frequency response over the range from 20 kHz to 1 MHz. The sensor has a finite aperture of 1 mm and is only sensitive to the surface displacement perpendicular to the sensing face. Therefore, the output voltage of the AE sensor is regarded to be linearly proportional to the surface displacement at the detection point. The influence of the AE sensor on the characteristics of the acoustic waves in both the time and frequency domains can be minimized. The installation and details of the AE sensor is shown in Fig. 4.

Experiments were carried out on a purpose-built test rig, as shown in Fig. 5. Particles are individually positioned at the top of a guiding tube by a tweezer and then released to impact onto the waveguide. The guiding tube has an inner diameter of 2 mm and is vertically held by the clamp of a retort stand. The distance between the bottom of the guiding tube and the flat plane of the waveguide is set to 5 mm. All particles are collected after colliding with the waveguide. In this way, tests are repeatable under each experimental condition.

A preamplifier (AMP-1BB-J, KRN Services) was used to provide power to the AE sensor and also a voltage gain of 28 dB over a bandwidth of 18 kHz - 2 MHz. As this study aims at investigating the propagation mechanism of the impact-induced AE signals along a waveguide, the experimental signals were collected at a much higher sampling rate than that usually required for on-line AE-based particle sizing so that the details of the acoustic waveforms were obtained. The AE signals were digitalized at a sampling rate of 5 MHz using a data acquisition device (PCI-6115, National Instruments). The length of the detected signals is 10 ms with a pretrigger time of 100 μs for experiments with the short waveguide and 30 ms with the same pretrigger time for experiments with the long waveguide. The characteristics of the detected AE signals were then processed and analysed on a personal computer.

3.3. Experimental conditions

Glass beads and steel beads with different diameters were utilised as test particles in this study. These two types of particles exhibit good physical properties, such as smooth surface, high homogeneity and regular shape, and are widely used as grinding and dispersing materials in many industrial processes. The experimental conditions are illustrated in Table 1. In order to obtain the AE signal arising from an impact event without the influence of a waveguide, the AE sensor was directly positioned under the guiding tube. Consequently, glass beads with a diameter of 0.6 mm can be dropped onto the sensing area of the AE sensor from a height of 35 mm. For the experiments with the short waveguide, glass beads with various diameters ranging from 0.4 mm to 1.0 mm were utilised to be dropped onto the waveguide. Three guiding tubes with different lengths (20 mm, 30 mm and 40 mm) were employed to allow the particles falling from different heights. In this way, different impact velocities were achieved. As the density of the steel bead is much higher than that of the glass bead, the resulting AE signal tends to saturate easily when a steel bead with a larger diameter collides with the waveguide. For this reason, only the steel beads with a diameter of 0.4 mm and 0.6 mm were used. Experiments were also performed with the long waveguide to make the particles impinging onto the waveguide at different locations. In this case, glass beads with a diameter of 0.8 mm were dropped from a height of 35 mm. All tests were repeated ten times under each experimental condition. The dropping height of the particle is subject to the characteristics of the AE sensor employed in this study. As a result, the range of impact velocities of the particles is different from that in the pneumatic conveying pipelines. However, as the force pulses generated from the collisions of particles with higher velocities on the waveguide have similar features with that occurring in free-fall experiments, the investigations into the wave propagation behaviour under such experimental conditions are still of significance.

4. RESULTS AND DISCUSSION

4.1. Analysis of typical AE signals

A typical AE signal from a single glass bead directly dropped onto the sensing area of the AE sensor is shown in Fig. 6. It is evident that two sharp peaks exist in the resulting AE signal, which is due to the loading and unloading of the contact force between the particle and the sensing area during the collision process. According to the Hertzian impact theory (Section 2.2), the loading and unloading stages for an impact event are inverses of each other. As a result, it is reasonable that the two peaks exhibit similar signal patterns with inverse directions. In addition, the two peaks are followed by a small damped oscillation with a short damping time of around 200 μs.

Fig. 7 shows an AE signal resulting from a single glass bead impacting onto the short waveguide. The diameter of the glass bead is 0.6 mm and the dropping height is 35 mm. As can be seen, after propagating along the waveguide, the acoustic signal has totally changed, which quickly reaches the peak amplitude at the beginning and then fades away with time. In comparison with the result in Fig. 6, the amplitude of the detected AE signal significantly decreases, which results from the strong attenuation of the elastic waves propagating along the waveguide. Meanwhile, the duration of the damping becomes much longer, mainly owing to the multiple reflections of the elastic waves during the propagation.

The propagation of the acoustic signal along a waveguide is generally in the form of guided waves, which exist simultaneously in symmetric and anti-symmetric modes [23]. In principle, there are infinite numbers of such guided wave modes. But the wave modes encountered in practical AE testing are usually the fundamental symmetric (S_0) mode and the fundamental anti-symmetric (A_0) mode [24, 25]. The acoustic waveforms detected at different sides of the short waveguide are plotted in Fig. 8. For clarity, the period of the waveforms is set to be 100 μs, which is large enough to allow the full development of the fundamental waves. It can be clearly seen that

the S_0-mode wave firstly arrives at around 10 μs as simultaneous upward and downward oscillation is observed at opposite sides of the waveguide. The propagation velocity of the S_0-mode wave is higher than that of the A_0-mode wave. Thus, it can be detected earlier by the AE sensor. Subsequently, the A_0-mode wave with a much higher amplitude arrives at around 20 μs, the oscillation of which shows similar patterns with the inverse phase. The discrepancies between the two acoustic waveforms detected at opposite positions are mainly due to the unsymmetrical geometry of the short waveguide.

The AE signal generated by a particle impact is of non-stationary nature. The Fourier transform returns all frequency components contained in the signal regardless of whether these frequencies cover the whole signal period or are just transient [26]. Therefore, it is inappropriate to process the AE signal using the conventional Fourier transform as the frequency characteristics of the AE signal change with time. In this study, the Choi-Williams distribution (CWD) was applied to investigate the time-frequency characteristics of the detected AE signal, which is an effective method for signals with complex frequency components [27]. The calculation of the CWD was conducted with the AGU-Vallen Wavelet software (Vallen Systeme Company) [28]. This is a free software to calculate the spectrogram of a waveform, which shows the wave intensity with a colour scale on a diagram of frequency versus time. The frequency resolution in the CWD-diagram is set at 1.221 kHz and the time resolution is 0.2 μs, corresponding to the sampling frequency in the experiments.

The CWD of the acoustic waveform detected at the side of the cylindrical surface in Fig. 8 is calculated, as shown in Fig. 9. In order to display the calculated results better, the full scale of the CWD-diagram only shows the frequencies below 500 kHz, as can be seen in Fig. 9(a). For the truncated scale of the CWD-diagram corresponding to the S_0-mode wave, frequencies up to 1000

kHz are displayed in Fig. 9(b), which is also consistent with the maximum operating frequency of the AE sensor. According to the arrival time of the waves with different modes, the resulting waveform is clearly dominated by the A_0-mode wave at a frequency of around 50 kHz from the full scale of the CWD-diagram. The magnitude of the calculated CWD corresponding to the S_0-mode wave is significantly smaller than that corresponding to the A_0-mode wave. The CWD of the S_0-mode wave is therefore invisible in Fig. 9(a). As can be seen in Fig. 9(b), the dominant frequency of the S_0-mode wave is about 450 kHz, which is much higher than that of the A_0-mode wave. This is in accordance with the propagation characteristics of the guided waves. The S_0-mode wave usually propagates at higher frequencies along the waveguide than the A_0-mode wave, which can be confirmed by the group-velocity dispersion curves of the guided waves [29].

4.2. Influence of different parameters

4.2.1 Particle size

The particle size has a significant influence on the impact process and thus greatly affects the resulting AE signal. During the experiments the AE sensor was attached to the cylindrical surface of the short waveguide and different sized glass beads were dropped from a height of 35 mm. The resulting acoustic waveforms are plotted in Fig. 10. As can be noticed, the amplitude of the detected waveforms increases with the particle size. This can be attributed to the reason that a larger particle tends to produce a greater contact force when colliding with a waveguide, resulting in a higher amplitude. It can be also found that although the increase of the signal amplitude is observed, the detected waveforms show highly similar tendencies with time. This result indicates that the particle size has a great influence on the amplitude rather than the signal pattern of the resulting AE signal.

4.2.2 Impact velocity

The impact velocity is another important parameter which influences the detected acoustic waveforms. With the AE sensor being fitted onto the cylindrical surface of the short waveguide, a 0.8-mm glass bead was dropped from a height of 25, 35 and 45 mm, respectively. The resulting waveforms are presented in Fig. 11. It can be seen that the signal amplitude generally shows an increasing trend with the dropping height due to the higher impact velocity. However, unlike the observation in Fig. 10, the signal pattern of the waveforms changes a lot with the various dropping heights. Especially, the waveform generated by the particle falling from a height of 45 mm becomes distorted at around 33 μs. A possible reason is that with the increase of the dropping height, the impact velocity of the particle grows, making the collision between the particle and the waveguide turn to be inelastic. For an inelastic collision, it still has the same elastic compression process as an elastic collision at the very beginning. It is only when the inelastic deformation occurs that the energy release during the collision changes, leading to the distortion of the resulting acoustic waveform. However, the determination of the exact time when the distortion takes place requires an explicit further understanding of impact dynamics and wave propagation theories, which is beyond the scope of the present study.

4.2.3 Material type

In order to investigate the influence of the material type on the detected AE signal, two types of particles with various diameters were dropped from a height of 35 mm. Experiments were performed with the short waveguide and the resulting acoustic waveforms were acquired via the AE sensor attached to the cylindrical surface of the waveguide. Fig. 12 illustrates the acoustic waveforms for different particle materials. As the density of the steel bead is larger than that of the glass bead, a greater contact force is generated during the collision. As a result, the waveforms

for steel beads have higher amplitudes than that for glass beads with the same diameters. Besides, the detected acoustic waveforms also keep relatively consistent in signal pattern.

4.2.4 Impact location

To demonstrate the influence of the impact location on the resulting AE signal, a glass bead with a diameter of 0.8 mm was dropped above different locations on the long waveguide from a height of 35 mm. The AE sensor was mounted onto the cylindrical surface of the long waveguide. The resulting acoustic waveform generated at the Position 3 is shown in Fig.13. As can be seen, the detected waveform using the long waveguide has a smaller amplitude compared with that using the short waveguide (Fig. 8). This is because the attenuation of the detected AE signal is much serious during the propagation due to the longer distance from the impact location to the sensor on long waveguide. Meanwhile, the signal pattern (both the S_0-mode and A_0-mode waves) also changes. For example, a longer S_0-mode waveform is clearly observed as the distance between the impact location and the AE sensor increases. When the elastic stress waves from the AE source propagate along a waveguide, the waveforms will broaden as a result of the dispersion effect, which becomes more obvious with a longer propagation distance. Meanwhile, the velocity of the S_0-mode wave is higher than that of the A_0-mode wave, making these two types of waves distinctively separated from each other after propagating along the waveguide.

The CWD of the acoustic waveform generated at the Position 3 was also calculated and is plotted in Fig. 14. It can be found that the dominant frequency in the waveform is about 34 kHz from the full scale of the CWD-diagram in Fig. 14(a). This shows that the A_0-mode wave generated using the long waveguide has lower dominant frequency than that using the short waveguide. The CWD-diagram of the S_0-mode wave is also illustrated in Fig. 14(b). As can be seen, the dominant frequency of the resulting S_0-mode wave is around 160 kHz, which is also

lower than that using the short waveguide. This manifests that a longer waveguide tends to decrease the dominant frequency of the detected AE signal. From the experimental results, it is concluded that the resulting AE signal significantly changes in both time and frequency domains using different waveguides.

The acoustic waveforms generated at other four positions on the long waveguide are depicted in Fig. 15. The distances (L) between the impact positions and the AE sensor are also given, respectively. Different impact positions mean different propagation distances of the waves, which eventually affect the signals detected by the AE sensor. It can be seen that the length of the S_0-mode wave shortens with the propagation distance. The S_0-mode wave also markedly changes in signal pattern, as there are two small fluctuations observed in the waveforms generated at Position 1 and 2, but only one in the waveforms generated at Position 4 and 5. Additionally, the signal patterns of the A_0-mode waves generated at different impact positions vary from each other due to the attenuation and reflection during the propagation. The amplitude of the resulting AE signal generally shows an increasing trend with a shorter propagation distance. However, the peak value of the waveforms generated at different positions has no significant change. Generally speaking, the impact location has influences on both the amplitude and pattern of the detected AE signal.

From the experimental results above, it can be seen that the AE signal arising from an impact event has completely lost fidelity after propagating along a waveguide, which brings challenges to infer the particle size information from the detected AE signals. The geometry of the waveguide affects the reflection, attenuation and dispersion of the AE signals during propagation. However, the design of the waveguide should ensure normal collisions of particles with the waveguide and minimize unnecessarily complex modal conversion of the acoustic waves to maintain the characteristics of the AE source. Different parameters during a collision also have different

influences on the resulting AE signals. Some parameters may greatly affect the result of particle size inversion. For example, the AE signals detected at different impact locations become stretched in varying degrees due to the different propagation distances. In this study, the propagation time of the S_0-mode wave increases by around 10 μs when the distance between the impact location and the AE sensor increases by 75 mm. If the impact location is far from the AE sensor, the AE signal will last for a long time, which increases the chance of overlapping impact signals. This issue becomes severer when the particle concentration is relatively high or the particle moves at a higher velocity. Therefore, although a longer waveguide is conducive to the acquisition of the AE signals, the length of the waveguide designed for on-line particle sizing should be within a reasonable range.

It is worth noting that, apart from the AE sensor, various elements used in the detection system also influence the resulting AE signal. For instance, the frequency response of the preamplifier should be flat over the frequency range of the AE signal being detected. Otherwise, the details of the original AE signal may be changed or lost, especially the characteristics in the frequency domain.

5. CONCLUSIONS

This paper has presented experimental investigations into the propagation behaviour of the impact-induced AE signal along a waveguide under different conditions. Two fundamental guided wave modes have been found in the resulting AE signal, which are the S_0-mode wave and the A_0-mode wave, respectively. The S_0-mode wave propagates with a faster velocity but lower amplitude than the A_0-mode wave. According to the CWD of the detected acoustic waveform, the dominant frequency of the S_0-mode wave was found to be higher than that of the A_0-mode wave, which are both affected by the length of the waveguide.

The experimental results obtained have also indicated that both the particle size and material type have little influence on the signal pattern of the detected acoustic waveform, but affect the signal amplitude. The impact velocity has significant impact on both the amplitude and pattern of the detected signal. Especially, when the particle collides with the waveguide from a higher dropping height, an obvious change in the signal pattern has been observed. In addition, the amplitude and the pattern of the resulting acoustic waveform are also affected by the impact location. However, the peak value of the waveform has no significant change with the impact location. In order to minimize the influence of the impact location on the detected AE signal and hence the chance of overlapping impact signals, the length of the waveguide should be within a reasonable range.

Further research will be conducted in the near future to investigate the propagation of AE signals resulting from simultaneous collisions of multiple particles along a waveguide, aiming to separate individual impact events and extract particle size information.

ACKNOWLEDGMENT

The authors would like to acknowledge the National Natural Science Foundation of China (No. 61573140) and the Fundamental Research Funds for the Central Universities (No. 2019MS021) for providing financial support for this research.

REFERENCES

[1] J. Boyd, J. Varley, The uses of passive measurement of acoustic emissions from chemical engineering processes, Chem. Eng. Sci. 56 (2001) 1749-1767.

[2] L. Jing, Z. Li, Y. Li, R. Murch, Channel characterization of acoustic waveguides consisting of straight gas and water pipelines, IEEE Access 6 (2018) 6807-6819.

[3] I. Ihara, D. Burhan, Y. Seda, Ultrasonic in-situ monitoring of solidification and melting behaviors of an aluminium alloy, IEEE Ultrason. Symp. 1 (2004) 541-544.

[4] L. Gao, Y. Yan, R. Carter, D. Sun, P. Lee, C. Xu, On-line particle sizing of pneumatically conveyed biomass particles using piezoelectric sensors, Fuel 113 (2013) 810-816.

[5] K. Prabakar, S. Rao, Pattern recognition analysis of acoustic emission signals propagated through a waveguide-A simulation study, Indian J. Pure Appl. Phys. 45 (2007) 900-905.

[6] D. Zakharov, S. Ptichkov, V. Shemyakin, Acoustic emission signal attenuation in the waveguide used in underwater AE testing, Proc. Eur. Conf. Non-Destr. Test. 50 (Moscow, Russia, 7-11 June 2010).

[7] Y. Hu, L. Wang, X. Huang, X. Qian, L. Gao, Y Yan, On-line sizing of pneumatically conveyed particles through acoustic emission detection and signal analysis, IEEE Trans. Instrum. Meas. 64 (2015) 1100-1109.

[8] A. Bastari, C. Cristalli, R. Morlacchi, E. Pomponi, Acoustic emissions for particle sizing of powders through signal processing techniques, Mech. Syst. Signal Process. 25 (2011) 901-916.

[9] G. Zhang, Y. Hu, Y. Yan, G. Zheng, On-line size measurement of pneumatically conveyed particles through acoustic emission sensing, Powder Technol. 353 (2019) 195-201.

[10] K. Ono, H. Cho, Rods and tubes as AE waveguides, J. Acoust. Emiss. 22 (2004) 243-252.

[11] J. Sikorska, J. Pan, The effect of waveguide material and shape on acoustic emission transmission characteristics Part 1: traditional features, J. Acoust. Emiss. 22 (2004) 264-273.

[12] J. Sikorska, J. Pan, The effect of waveguide material and shape on acoustic emission transmission characteristics Part 2: frequency and joint-time-frequency characteristics, J. Acoust. Emiss. 22 (2004) 274-287.

[13] M. Hamstad, Small diameter waveguide for wideband acoustic emission, J. Acoust. Emiss. 24 (2006) 234-247.

[14] L. Vergeynst, M. Sause, M. Hamstad, K. Steppe, Deciphering acoustic emission signals in drought stressed branches: the missing link between source and sensor, Front. Plant Sci. 6 (2015) 494.

[15] A. Zelenyak, M. Hamstad, M. Sause, Modeling of acoustic emission signal propagation in waveguides, Sens. 15 (2015) 11805-11822.

[16] M. Sause, Investigation of pencil-lead breaks as acoustic emission sources, J. Acoust. Emiss. 29 (2011) 184-196.

[17] D. Buttle, S. Martin, C. Scruby, Particle sizing by quantitative acoustic emission, Res. Nondestruct. Eval. 3 (1991) 1-26.

[18] G. Kocur, Deconvolution of acoustic emissions for source localization using time reverse modeling, J. Sound Vib. 387 (2017) 66-78.

[19] G. Zheng, Y. Yan, Y. Hu, W. Zhang, L. Yang, L. Li, Mass flow rate measurement of pneumatically conveyed particles through acoustic emission detection and electrostatic sensing, Proc. IEEE Int. Instrum. Meas. Technol. Conf. (Dubrovnik, Croatia, 25-28 May, 2020).

[20] R. Laschimke, M. Burger, H. Vallen, Acoustic emission analysis and experiments with physical model systems reveal a peculiar nature of the xylem tension, J. Plant Physiol. 163 (2006) 996-1007.

[21] G. Mclaskey, S. Glaser, Acoustic emission sensor calibration for absolute source measurement, J. Nondestruct. Eval. 2 (2012) 157-168.

[22] G. Mclaskey, S. Glaser, Hertzian impact: Experimental study of the force pulse and resulting stress waves, J. Acoust. Soc. Am. 128 (2010) 1087-1096.

[23] S. Pant, J. Laliberte, M. Martinez, Structural health monitoring (SHM) of composite aerospace structures using lamb waves, Proc. Int. Conf. Compos. Mater. (Montreal, Canada, 28 July-2 August, 2013).

[24] K. Ono, An experimental study of acoustic emission waveguides, J. Acoust. Emiss. 34 (2017) 12-52.

[25] M. Sause, M. Hamstad, S. Horn, Finite element modelling of conical acoustic emission sensors and corresponding experiments, Sens. Actuators, A 184 (2012) 64-71.

[26] A. Terchi, Y. Au, Acoustic emission signal processing, Meas. Control 34 (2001) 240-244.

[27] M. Hamstad, Comparison of wavelet transform and Choi-Williams distribution to determine group velocities for different acoustic emission sensors, J. Acoust. Emiss. 26 (2008) 40-59.

[28] M. Sause, S. Horn, Simulation of lamb wave excitation for different elastic properties and acoustic emission source geometries, J. Acoust. Emiss. 28 (2010) 142-154.

[29] P. Zhang, Z. Tang, F. Lv, K. Yang, Numerical and experimental investigation of guided wave propagation in a multi-wire cable, Appl. Sci. 9 (2019) 1028.

List of Figures:

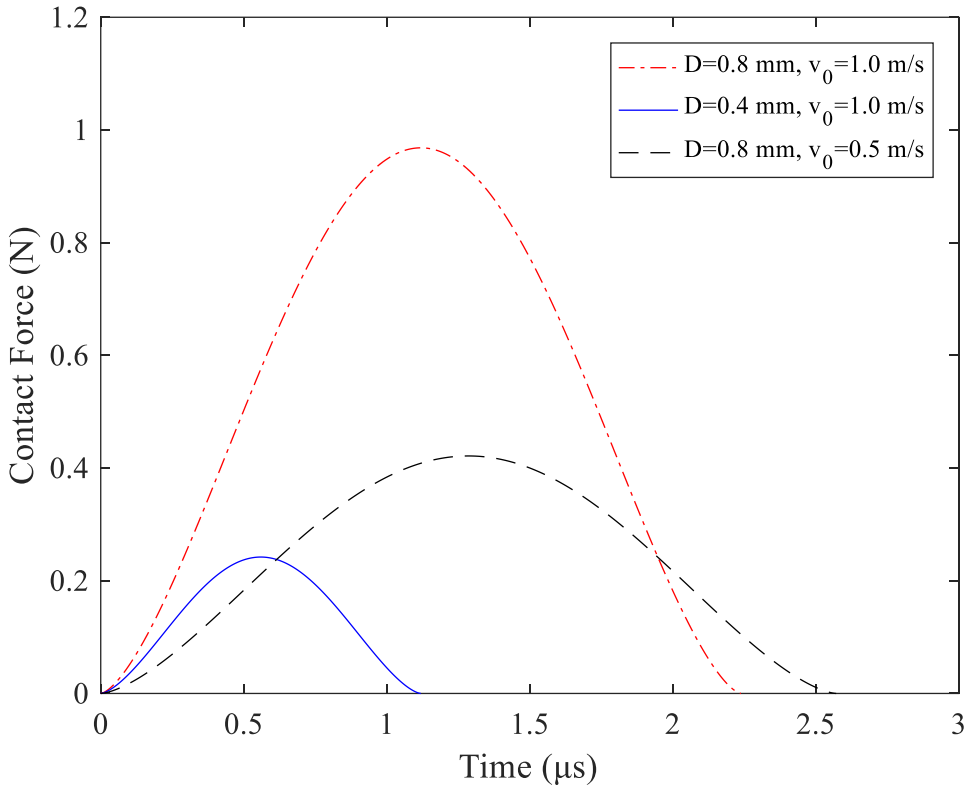

Fig. 1. Force-time curves according to the Hertzian impact theory under different conditions (glass bead).

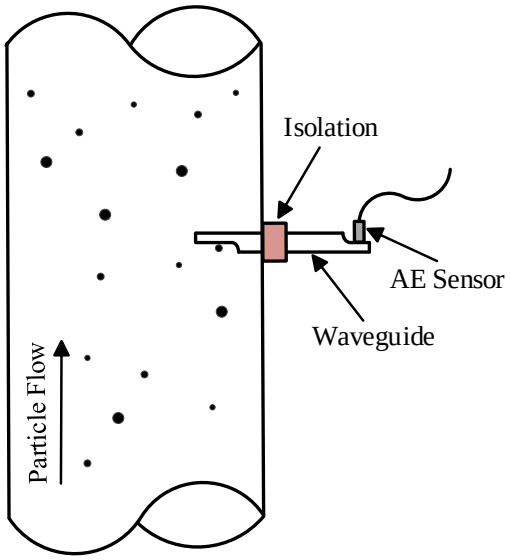

Fig. 2. Schematic illustration of the AE sensing arrangement.

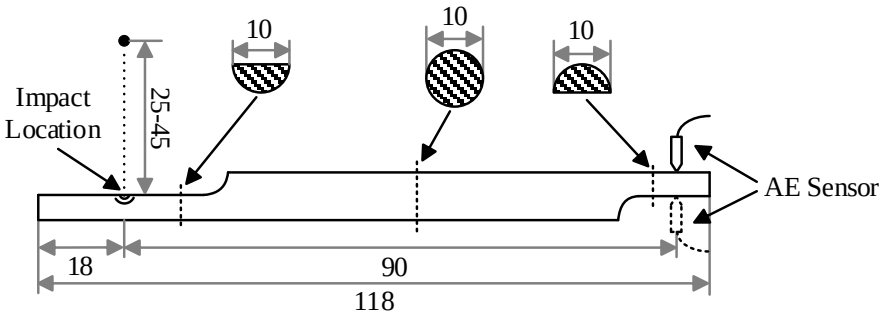

(a) Short waveguide

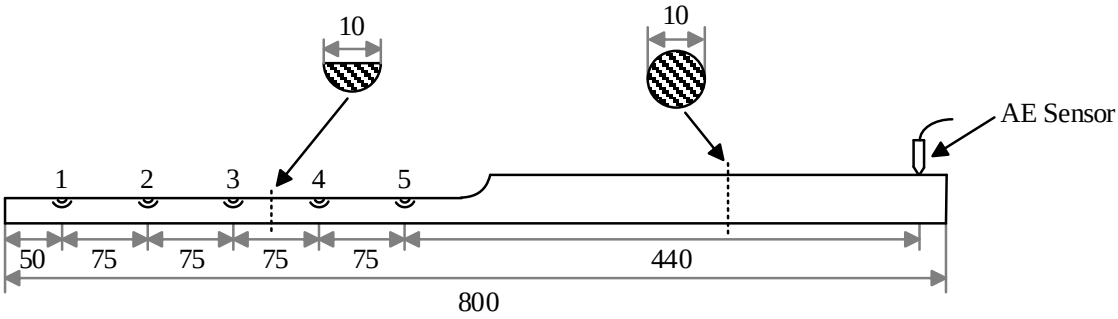

(b) Long waveguide

Fig. 3. Schematic diagrams of the waveguides and the installation of the AE sensor (Unit: mm).

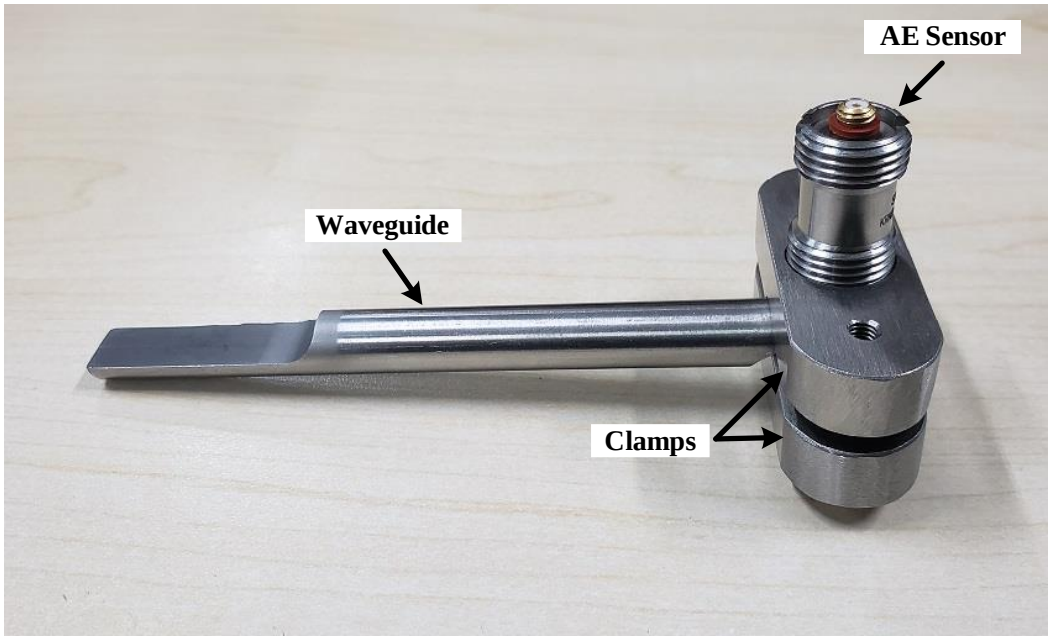

(a) Installation of the AE sensor on the waveguide

(b) Details of the AE sensor

Fig. 4. Installation and details of the AE sensor.

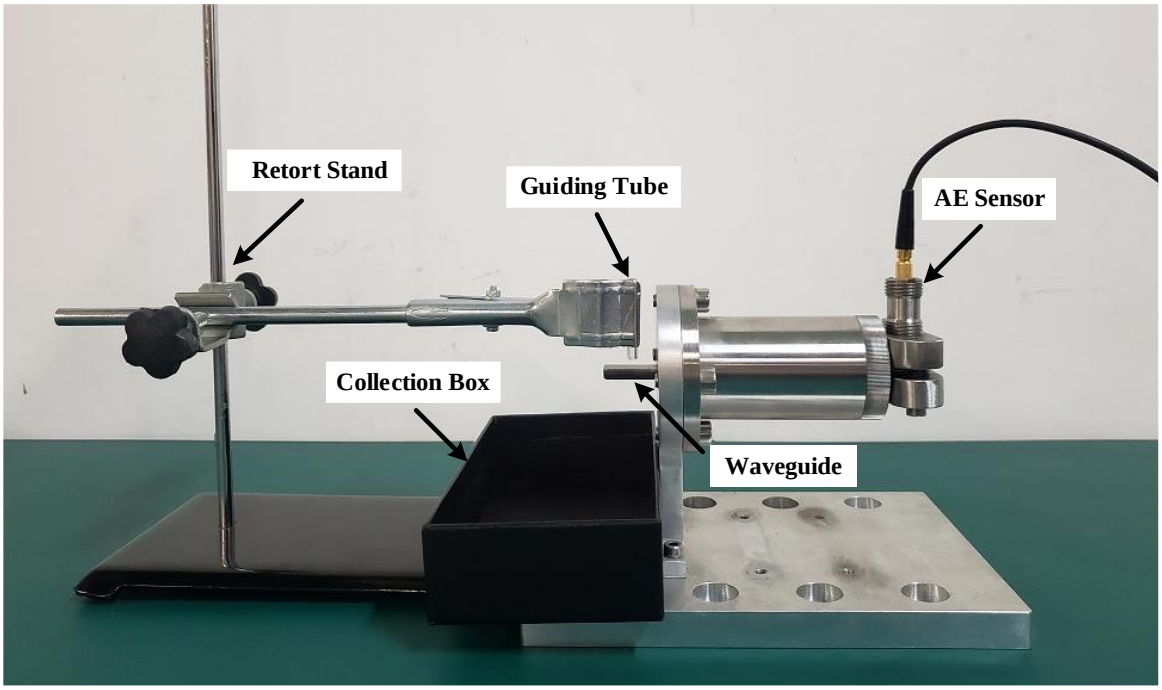

Fig. 5. Experimental setup.

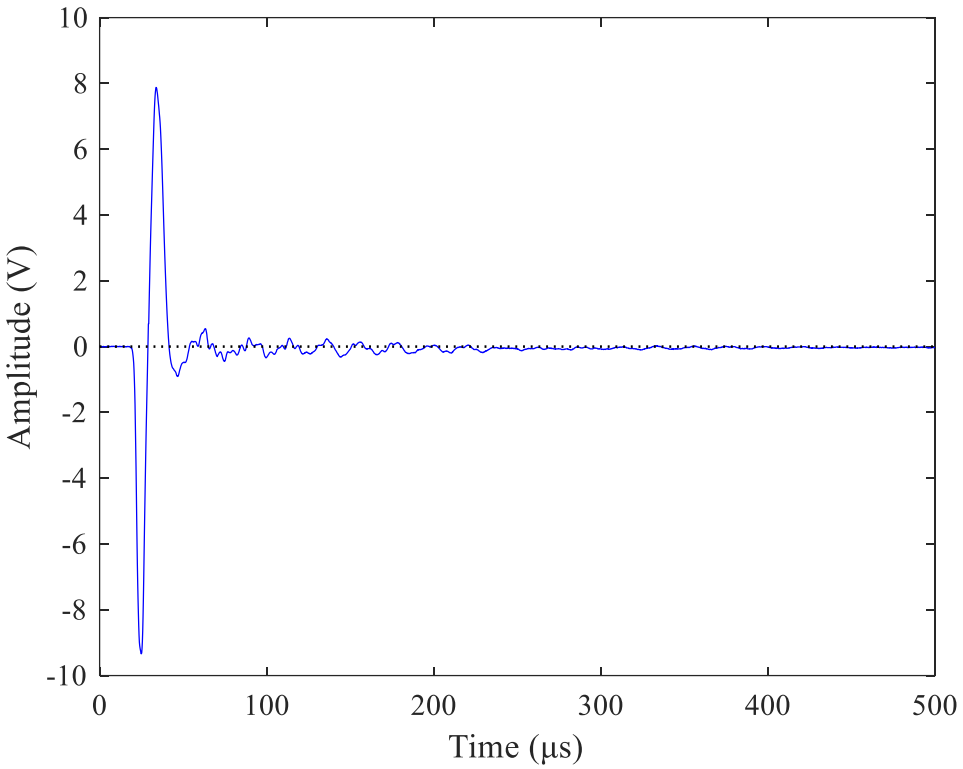

Fig. 6. A typical AE signal from a single particle directly impacting onto the sensing area of the AE sensor (glass bead, *D*=0.6 mm, *H*=35 mm).

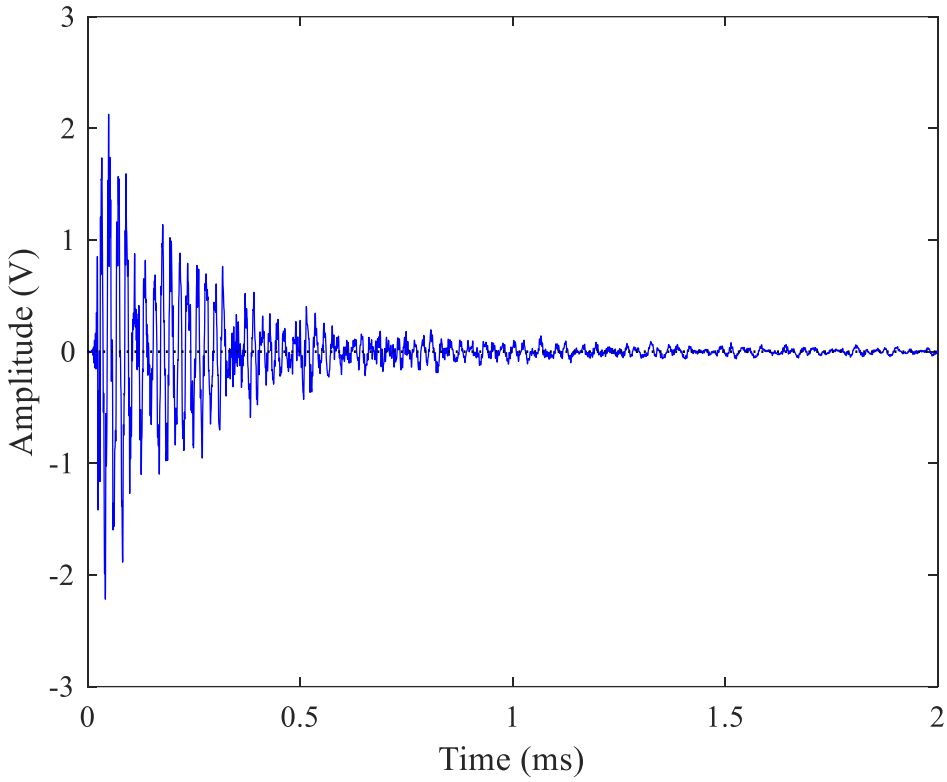

Fig. 7. A typical AE signal from a single particle impacting onto the short waveguide (glass bead, D=0.6 mm, H=35 mm).

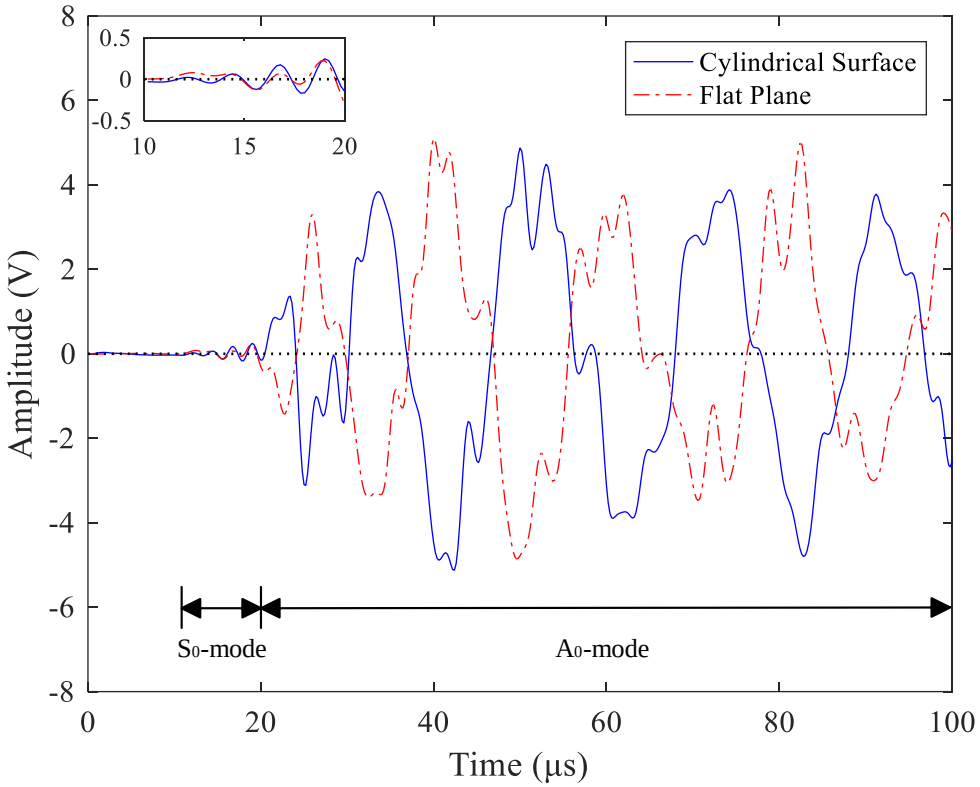

Fig. 8. Acoustic waveforms detected at different sides of the short waveguide (glass bead, *D*=0.8 mm, *H*=35 mm).

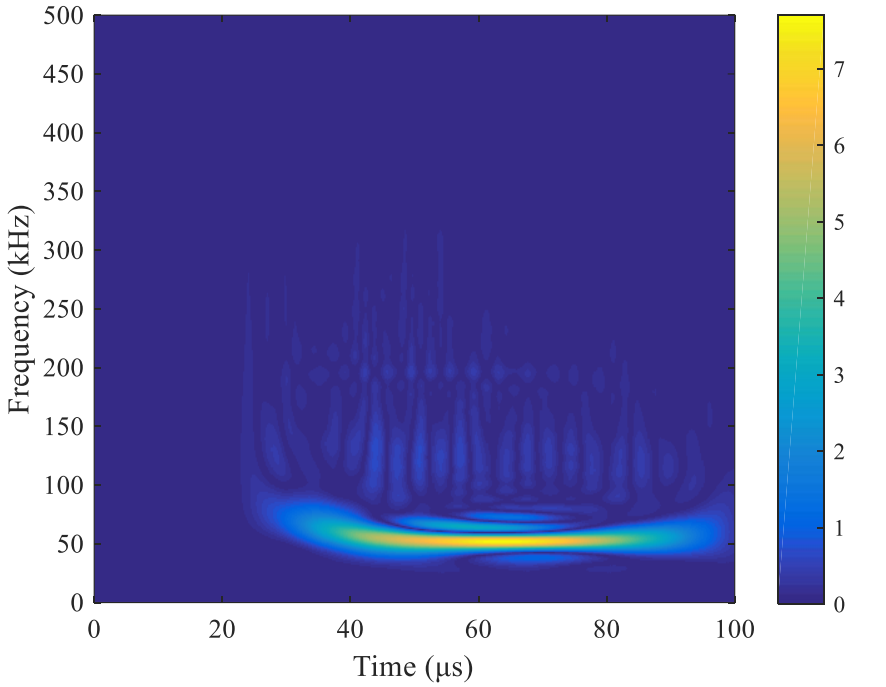

(a) Full scale

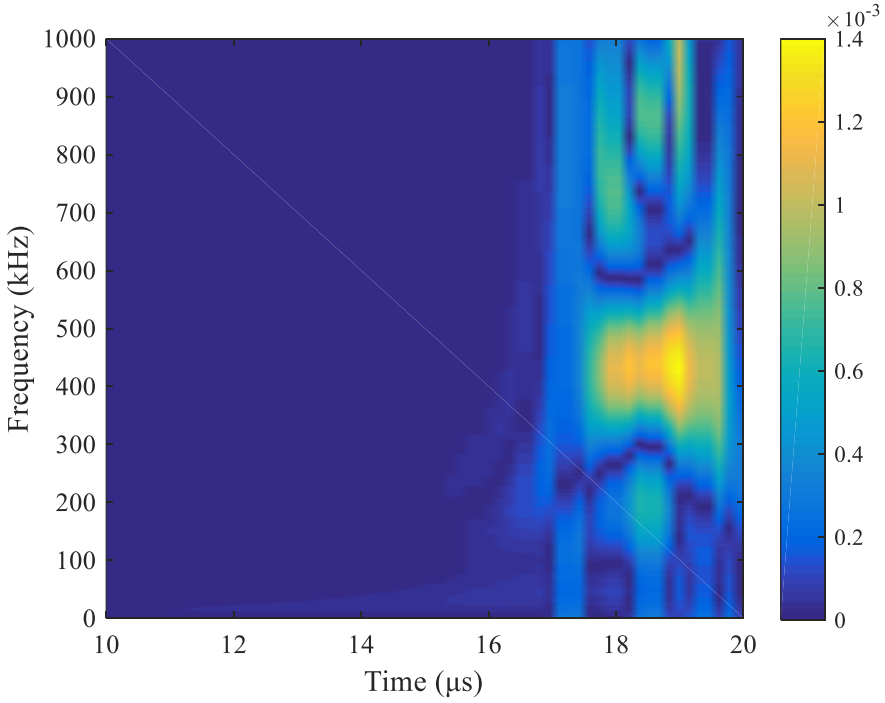

(b) Truncated scale

Fig. 9. CWD of the acoustic waveform detected at the side of the cylindrical surface in Fig. 8.

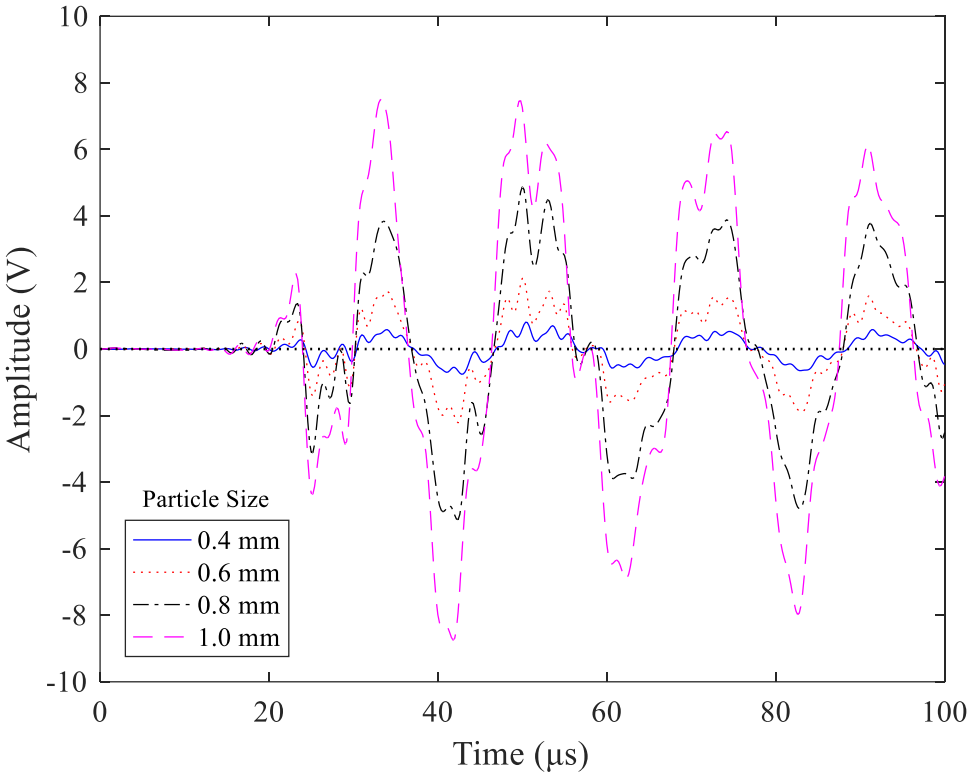

Fig. 10. Acoustic waveforms for different particle sizes (glass bead, *H*=35 mm, short waveguide, cylindrical surface).

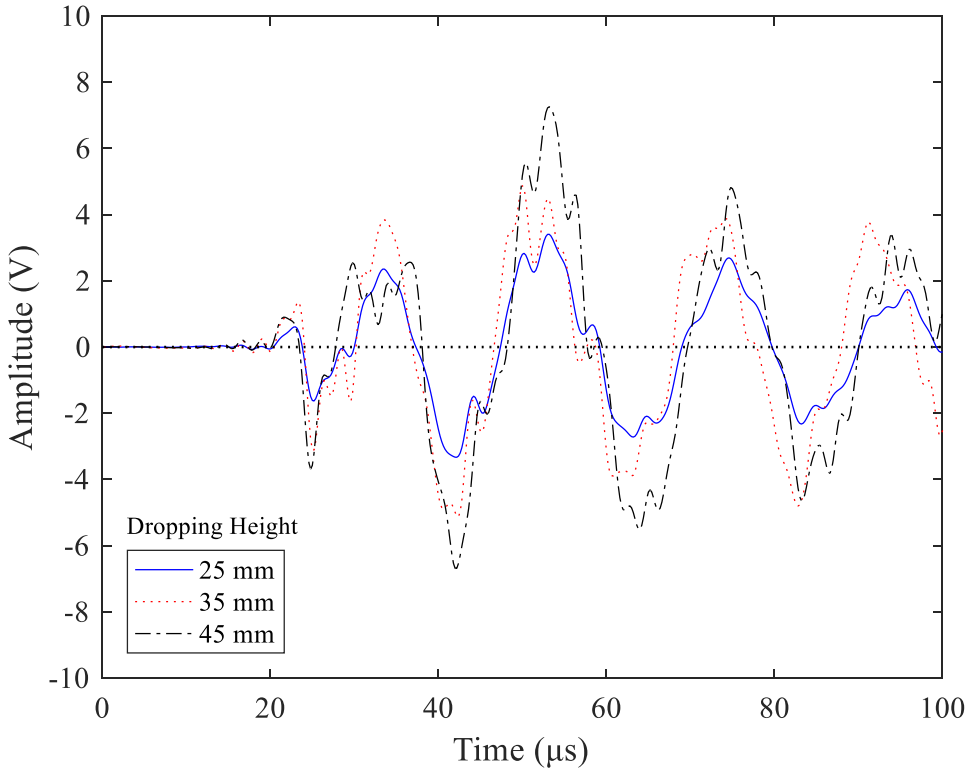

Fig. 11. Acoustic waveforms for different dropping heights (glass bead, *D*=0.8 mm, short waveguide, cylindrical surface).

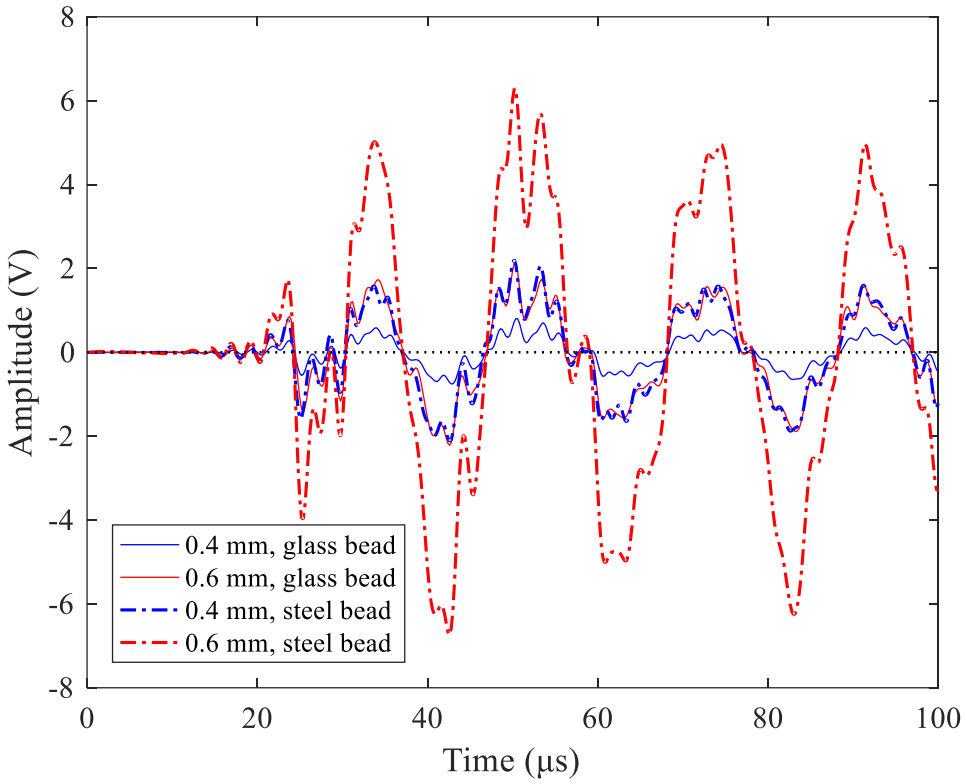

Fig. 12. Acoustic waveforms for different particle materials (*H*=35 mm, short waveguide, cylindrical surface).

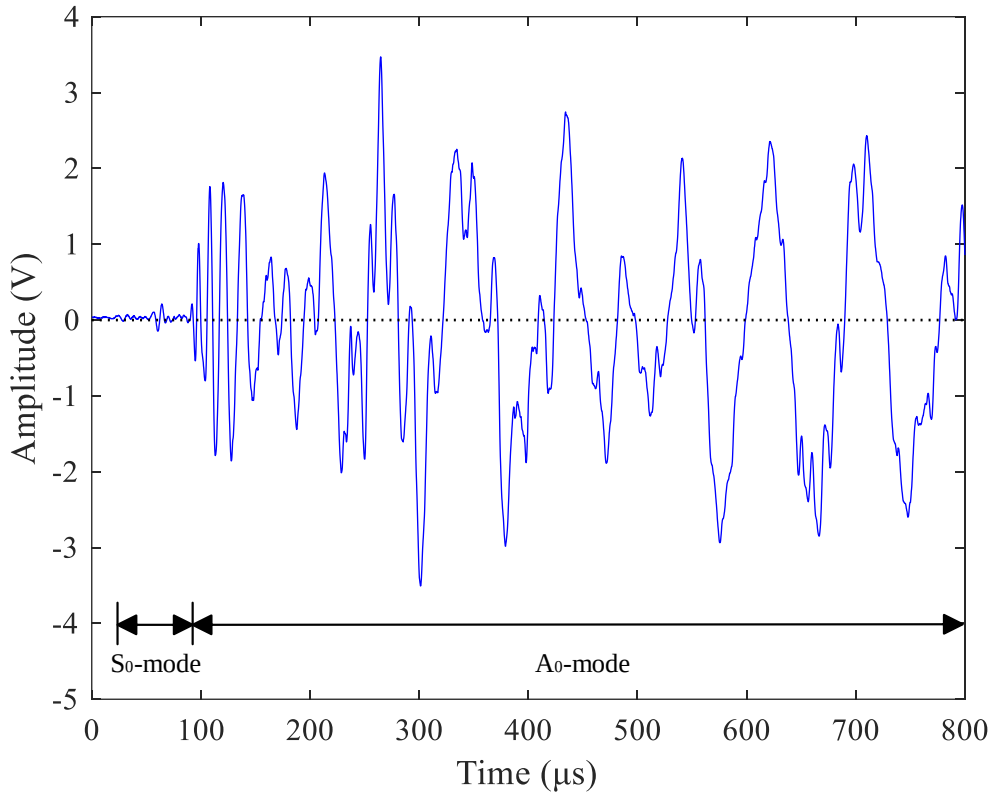

Fig. 13. Resulting acoustic waveforms generated at Position 3 on the long waveguide (glass bead, *D*=0.8 mm, *H*=35 mm, cylindrical surface).

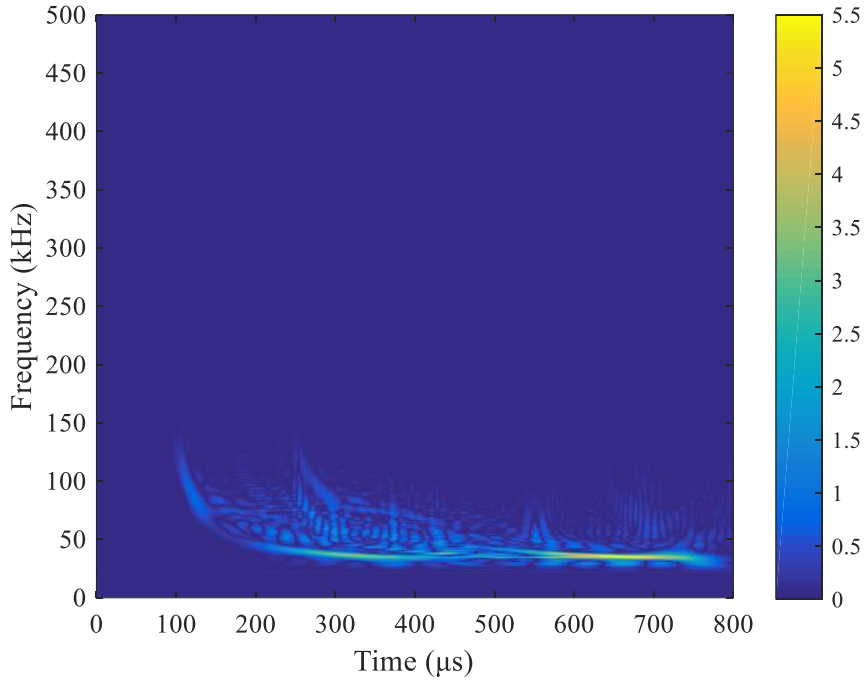

(a) Full scale

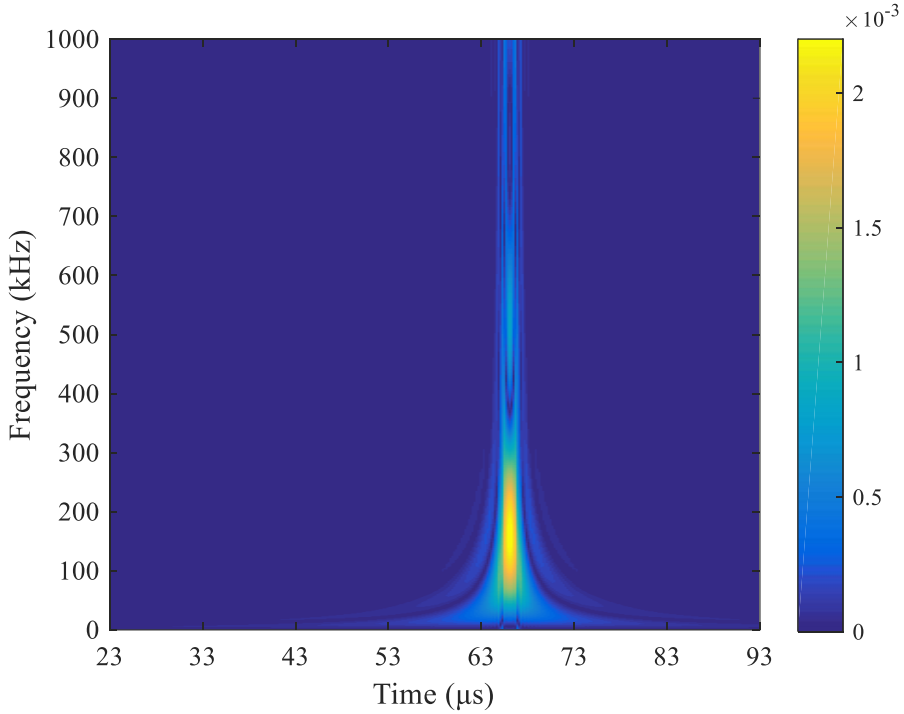

(b) Truncated scale

Fig. 14. CWD of the acoustic waveform in Fig. 13.

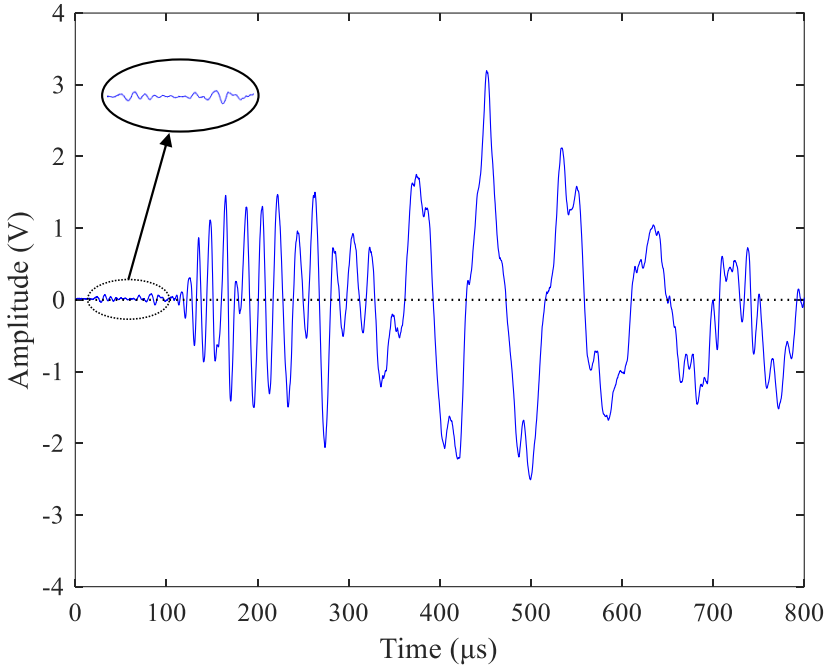

(a) Position 1 (L=740 mm)

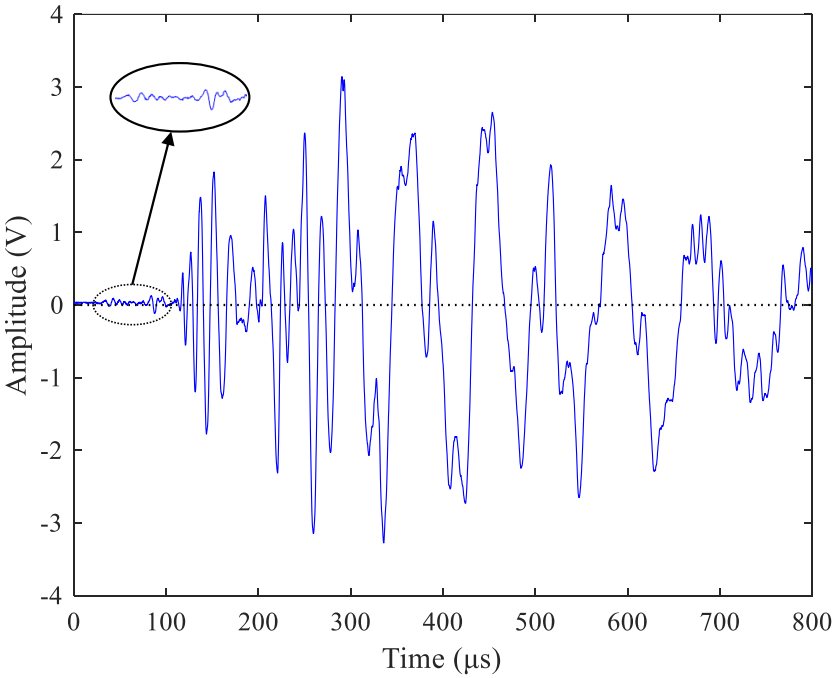

(b) Position 2 (L=665 mm)

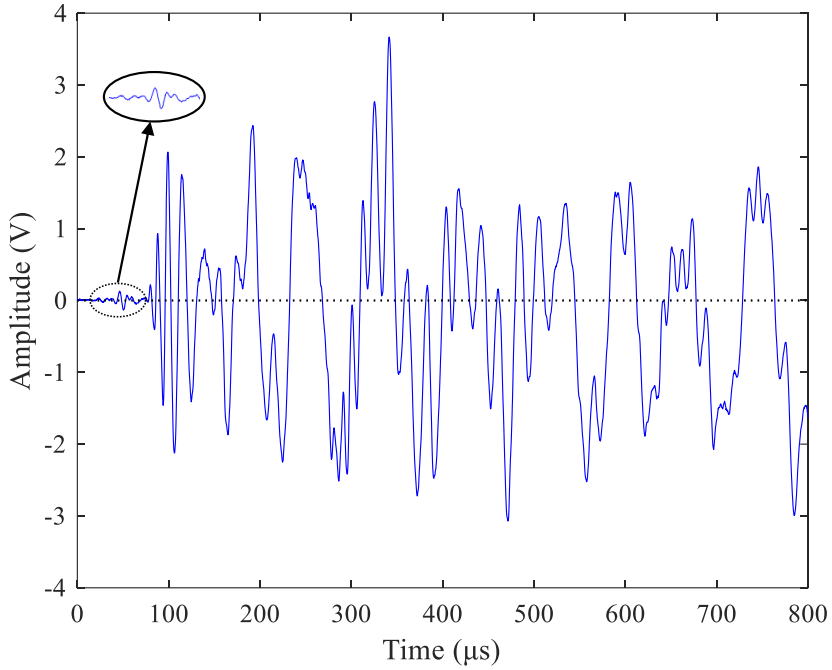

(c) Position 4 (L=515 mm)

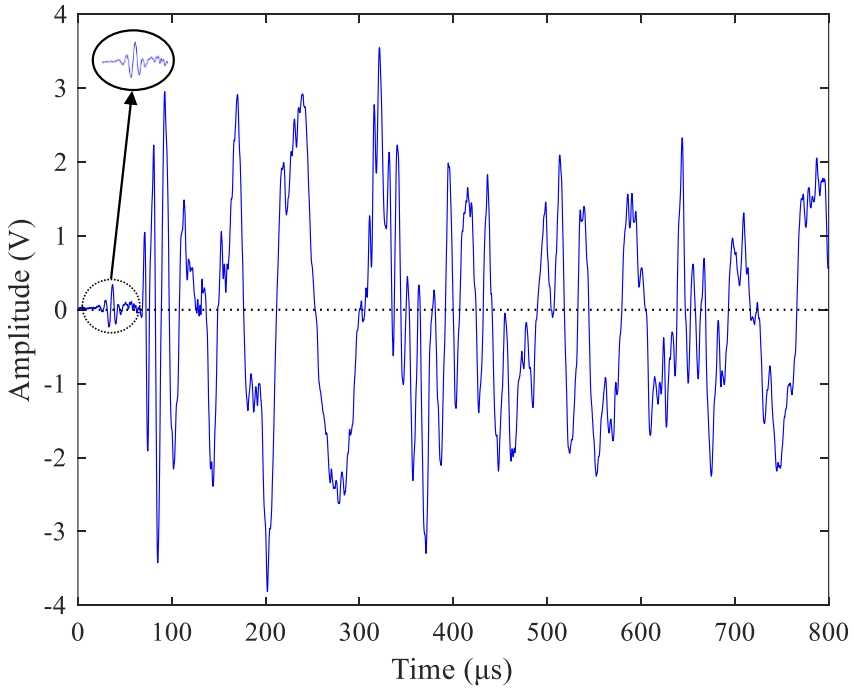

(d) Position 5 (L=440 mm)

Fig. 15. Acoustic waveforms generated at different positions on the long waveguide (glass bead, D=0.8 mm, H=35 mm).

List of Tables:

Table 1. Experimental conditions

Waveguide	Particle type	Particle diameter (D) (mm)	Dropping height (H) (mm)
No waveguide	Glass beads	0.6	35
Short waveguide	Glass beads	0.4	35
		0.6	35
		0.8	25/35/45
		1.0	35
	Steel beads	0.4	35
		0.6	35
Long waveguide	Glass beads	0.8	35